The Impact of Beamforming on Energy Correlation in mm-Wave Wirelessly Powered Networks

Na Deng*† and Martin Haenggi‡
*School of Information & Communication Engineering, Dalian University of Technology, Dalian, 116024, China
†National Mobile Communications Research Laboratory, Southeast University, Nanjing, 210096, China
‡Dept. of Electrical Engineering, University of Notre Dame, Notre Dame, IN, 46556, USA
Email:*†dengna@dlut.edu.cn, ‡mhaenggi@nd.edu

***Abstract*—This paper studies the spatial correlation of the energy harvested from a Poisson field of millimeter-wave (mm-wave) RF power sources which employ beamforming techniques to transfer energy directionally. In particular, each node harvests and stores energy from its nearest RF transmitter and uses it to power the information transmission. Under this setup, we show how the actual point process of nodes that successfully harvest energy looks visually and provide an accurate characterization of its density and pair correlation function theoretically. Surprisingly, it turns out that the process of the energized nodes exhibits repulsive correlations for small distances which wears off as the distance increases. Therefore, we further approximate the energized point process with a fitted β-Ginibre point process, which is shown to provide a good approximation of the success probability in the information transmission. A useful insight is that there are energy correlations caused by the directional energy transfer, which should be reflected accurately in modeling the active mm-wave RF-powered nodes.**

I. Introduction

Wireless energy transfer (WET) is a key enabling technology in realizing low-powered and self-sustainable wireless communication networks, especially for the Internet of Things, where billions of devices and sensors will be deployed, thus powering or charging them has become a crucial issue in next-generation networks. Meanwhile, as one of the main components of the emerging 5G, millimeter-wave (mm-wave) communication is expected to play an important role in accommodating the explosive growth of traffic demands and devices. Moreover, the very short wavelength makes it possible to adopt relatively large antenna arrays at the transceivers to achieve substantial array gains via various beamforming techniques. However, unlike the conventional sub-6 GHz systems, mm-wave signals experience high propagation losses and are susceptible to blockages [1]. While bringing about huge benefits, the integration of RF-based energy harvesting in mm-wave band also triggers new problems and challenges.

One of the key challenges in the application of WET over mm-waves is the lack of tractable models for analysis and design of such networks. As a consequence, stochastic geometry models for wirelessly powered networks have recently received widespread attention due to their capability of capturing the irregularity and variability of the node configurations in real networks and providing theoretical insights [2–4]. For the sake of analytical tractability, most existing studies on the joint consideration of mm-wave and WET use independent Poisson point processes (PPPs) as models for both RF transmitters and the active RF-powered nodes that successfully harvest energy and use it to power their information transmission [2–5]. However, modeling the active RF-powered nodes as a PPP means that whether a node succeeds in harvesting energy is independent of whether a nearby node succeeds, which does not seem realistic. Nodes powered by different RF transmitters with directional beams are likely to exhibit spatial correlation, e.g., the RF-powered nodes residing in the Voronoi cells of different RF transmitters usually exhibit repulsion. Therefore, it is important to explore tractable models for the energized nodes, i.e., the nodes that successfully harvest energy from mm-wave RF transmitters, accounting for the spatial correlation, and analyze the corresponding effect on the communication performance.

Different from the positive energy correlation shown in our previous work [6] with omni-directional energy transfer, in this paper we explore the impact of beamforming on the energy correlation in wirelessly powered networks over mm-wave bands, where the energy correlation corresponds to the spatial correlation of nodes that successfully harvest enough energy from mm-wave RF transmitters. The mm-wave RF transmitters employ beamforming techniques to transfer energy directed to the locations of certain RF-powered nodes. Under this setup, the active RF-powered nodes in the information transmission phase form a new point process, termed the *beamforming-based energized point process* (BEPP). To characterize the spatial correlation of the BEPP, we derive the first- and second-order (pair correlation function) statistics. Interestingly, it is shown that the BEPP exhibits repulsion for small inter-node distances and such correlation gradually recedes until it tends to zero or even turns positive as the distance increases. To assess the effect of such spatial correlation on the communication performance, we further use a fitted β-Ginibre point process (β-GPP) [7] to approximate the BEPP, which turns out to provide a good approximation of the transmission success probability.

II. System model

A. Network Model

We consider a mm-wave network powered solely by mm-wave RF transmitters, where the locations of RF transmitters follow a point process Φ_{p}. Based on the point process Φ_{p},

we model the locations of the RF-powered nodes as a point process on $\mathbb{R}^2$, which is denoted by $\Phi_{\rm d}$ and defined as follows

$$\Phi_{\rm d} \triangleq \{x \in \Phi_{\rm p} \colon U(V_x)\}, \tag{1}$$

where V_x is the Voronoi cell of x, and $U(B)$, $B \subset \mathbb{R}^2$ presents a point chosen uniformly at random from B which is independent for different B and independent from everything else. This model is suitable for a fully loaded wirelessly powered network, where each RF-powered node harvests energy from its nearest RF transmitter and each RF transmitter is equipped with a directional antenna array synthesizing a highly directional energy beam pointing to a RF-powered node. Hence, the densities of $\Phi_{\rm d}$ and $\Phi_{\rm p}$ are the same, i.e., $\lambda_{\rm d} = \lambda_{\rm p}$. Under this setup, we formally define the BEPP, denoted by $\Phi_{\rm e}$, which is formed by the mm-wave RF-powered nodes that succeed in harvesting enough energy from directional energy transfer beams. Obviously, we have $\Phi_{\rm e} \subset \Phi_{\rm d}$.

Definition 1 (Beamforming-based energized point process, BEPP). *Let $\Phi_{\rm p}$ be the point process of RF transmitters and $\Phi_{\rm d}$ be the point process of performing mm-wave energy harvesting from $\Phi_{\rm p}$. The beamforming-based energized point process $\Phi_{\rm e}$ is defined as*

$$\Phi_{\rm e} \triangleq \{x \in \Phi_{\rm d} \colon E(x, \Phi_{\rm p}) = 1\}, \tag{2}$$

where E is the energy indicator function describing whether enough energy can be harvested from $\Phi_{\rm p}$ at location x.

In this paper, $\Phi_{\rm p}$ is assumed to be a homogeneous PPP of density $\lambda_{\rm p}$. As a result, $\Phi_{\rm d}$ is identical to the user point process of type I in [8], which also provides a good approximation of the pair correlation function for $\Phi_{\rm d}$, given by

$$g_{\rm d}(r) \approx 1 - e^{-(9/4)\sqrt{\lambda_{\rm d}} r} + (1/2)\lambda_{\rm d} r^2 e^{-(5/4)\lambda_{\rm d} r^2}, \tag{3}$$

and the distance distribution between the RF-powered node and its associated RF transmitter is accurately approximated by the density function [8]

$$f(r) \approx 2(13/10)\lambda_{\rm p} \pi r e^{-(13/10)\lambda_{\rm p} \pi r^2}. \tag{4}$$

A realization of such a mm-wave wirelessly powered network modeled with $\Phi_{\rm p}$, $\Phi_{\rm d}$ and $\Phi_{\rm e}$ portrayed by a Voronoi tessellation is given in Fig. 1.

B. mm-Wave Energy Harvesting Model

Since the harvested energy depends on the aggregate received signal strength at the receiver, we consider an energy harvesting model that includes the practical factors in the mm-wave propagation environment, namely the blockage and the large beamforming gain from directional antenna arrays. To capture the blockage effect, the line-of-sight (LOS) ball model [9] is adopted, where the LOS probability of mm-wave propagation channel between two nodes with separation d is

$$P_{\rm LOS}(d) = \mathbf{1}(d < R_{\rm B}), \tag{5}$$

where $\mathbf{1}(\cdot)$ is the indicator function, and $R_{\rm B}$ is the maximum length of a LOS propagation channel. Due to the severe attenuation over mm-waves, the power of NLOS signals is negligible [10]. Thus, for a RF-powered node located at x, the relevant RF transmitters are denoted by $\tilde{\Phi}_{\rm p} = \Phi_{\rm p} \cap b(x, R_{\rm B})$, where $b(x, R_{\rm B})$ is a disk centered at x with radius $R_{\rm B}$. The path loss function with distance r is

$$\ell(r) = \begin{cases} r^{-\alpha}, & r \le R_{\rm B} \\ 0, & r > R_{\rm B}, \end{cases} \tag{6}$$

where α is the path loss exponent with $\alpha \in [1.9, 2.5]$.

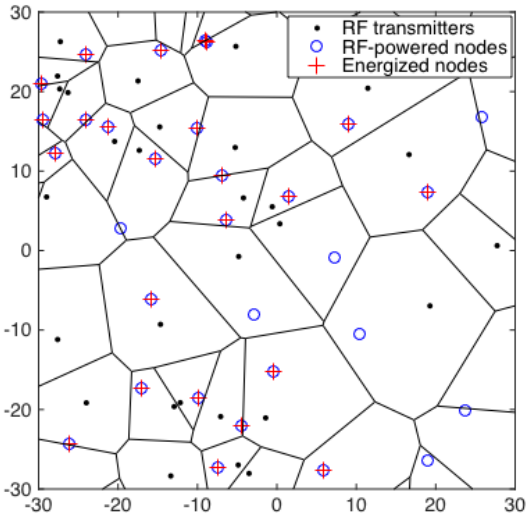

Fig. 1. A Voronoi network topology, where each mm-wave RF transmitter energizes the RF-powered node residing in its Voronoi region.

We assume that all nodes in mm-wave networks are equipped with uniform linear arrays (ULA), and analog directional beamforming technique is applied to overcome the severe attenuation in the mm-wave bands. For the ULA composed of N antennas, the actual antenna pattern is expressed as [10]

$$G_{\rm act}(\varphi) = \frac{\sin^2(\pi N \varphi)}{N \sin^2(\pi \varphi)}, \tag{7}$$

where $\varphi = \frac{d}{\rho}\cos\phi$ is the cosine direction corresponding to the physical angle of departure (AoD) ϕ, termed as the spatial AoD, with d and ρ representing the antenna spacing and wavelength, respectively. The configuration of $d = \rho/2$ is usually set to enhance the directionality of the beam and avoid grating lobes, and thus we have $\varphi \in [-0.5, 0.5]$. Due to the sine terms, the actual pattern is not analytically tractable, and thus a normalized flat-top antenna model [11] is adopted to approximate the actual antenna pattern. It is given by

$$G_x(\varphi) = \begin{cases} G_{x,{\rm m}}, & \text{if } |\varphi| \le w_{x,{\rm m}}/2 \\ G_{x,{\rm s}}, & \text{otherwise}, \end{cases} \tag{8}$$

where x denotes the node with the antenna size N_x, $G_{x,{\rm m}}$ is the maximum array gain, $w_{x,{\rm m}}$ is chosen as the half-power beamwidth (HPBW), and $G_{x,{\rm s}}$ is chosen to satisfy $\int_{-0.5}^{0.5} G_x(\varphi){\rm d}\varphi = 1$ (as in (7)). Hence, we have $G_{x,{\rm m}} = N_x$, $w_{x,{\rm m}} = 2G_{\rm act}^{-1}(N_x/2)$, and $G_{x,{\rm s}} = (1 - w_{x,{\rm m}}G_{x,{\rm m}})/(1 -$

$w_{x,\mathrm{m}}$). It is assumed that the spatial AoD between a RF-powered node and its associated RF transmitter φ is uniformly distributed in $[-0.5, 0.5]$ and thus the spatial AoD from other RF transmitters to this RF-powered node is also uniformly distributed in $[-0.5, 0.5]$, as proven in [10]. For a non-associated transmitter-receiver pair x and y, the total antenna array gain denoted by $G_{xy} = G_x(\varphi_x)G_y(\varphi_y)$ is a discrete random variable under the normalized flat-top antenna model, where the probability mass function is given by

$$G_{xy} = \begin{cases} G_1 = G_{x,\mathrm{m}}G_{y,\mathrm{m}}, & \text{w.p. } q_1 = w_{x,\mathrm{m}}w_{y,\mathrm{m}} \\ G_2 = G_{x,\mathrm{m}}G_{y,\mathrm{s}}, & \text{w.p. } q_2 = w_{x,\mathrm{m}}w_{y,\mathrm{s}} \\ G_3 = G_{x,\mathrm{s}}G_{y,\mathrm{m}}, & \text{w.p. } q_3 = w_{x,\mathrm{s}}w_{y,\mathrm{m}} \\ G_4 = G_{x,\mathrm{s}}G_{y,\mathrm{s}}, & \text{w.p. } q_4 = 1-q_1-q_2-q_3, \end{cases} \tag{9}$$

and the specific expression is determined by the antenna sizes of x and y. For the associated transmitter-receiver pair, we assume that both nodes know the exact direction and align their beams to obtain the maximum antenna array gain G_1. Denote N_p and N_d by the number of antenna elements of RF transmitters and RF-powered nodes, respectively. The transmit power of each RF transmitter is set to one. Using the linear energy harvesting model and neglecting the small-scale fading, the harvested energy $\varepsilon(x, \Phi_\mathrm{p})$ at x is quantified as

$$\varepsilon(x, \Phi_\mathrm{p}) = G_1\ell(y_0 - x) + \sum\nolimits_{y\in\Phi_\mathrm{p}^!} G_{yx}\ell(y - x), \tag{10}$$

where $\Phi_\mathrm{p}^! = \Phi_\mathrm{p}\backslash\{y_0\}$ denotes the non-associated RF transmitters for the RF-powered node x, and G_{yx} is the total antenna array gain between the transmitter-receiver pair y and x. Therefore, in this model, we have

$$E(x, \Phi_\mathrm{p}) = \mathbf{1}(\varepsilon(x, \Phi_\mathrm{p}) \geq \xi), \tag{11}$$

where ξ is the energy threshold.

Fig. 2 shows a comparison between realizations of the BEPP and the PPP with the same density. It is observed that the spatial distribution of the active RF-powered nodes exhibits repulsion relative to the PPP.

C. Communication Model

For simplicity, we assume that wireless energy transfer and information transmission adopt different frequency bands to avoid the mutual interference, and a time-switched "harvest-then-transmit" strategy is considered. Firstly, each RF-powered node is associated with its nearest RF transmitter and performs energy harvesting based on the directional beamforming technique. Then, if the harvested energy exceeds the predefined energy threshold, the RF-powered node becomes active and transmits a message to its dedicated receiver. Each RF-powered node is assumed to be battery-less and the instantaneously harvested energy from the RF transmitter is utilized to supply its operation. Furthermore, the dedicated receiver is assumed to be located at distance r_d from its transmitter (i.e., the active RF-powered node) in a random orientation. Similar to the energy transfer phase, the transmit power is set to one, and each receiver is also equipped with a ULA composed of N_r antennas and adopting analog beamforming.

TABLE I. Symbols and descriptions

Symbol	Description	Default
λ_p	The density of mm-wave RF transmitters	0.01
α	The path loss exponent	2.5
R_B	The radius of the LOS ball model	100
N_x	The antenna size of node x	8
ξ	The energy threshold	1
r_d	The communication distance	5
β	The fitted parameter of β-GPP	N/A

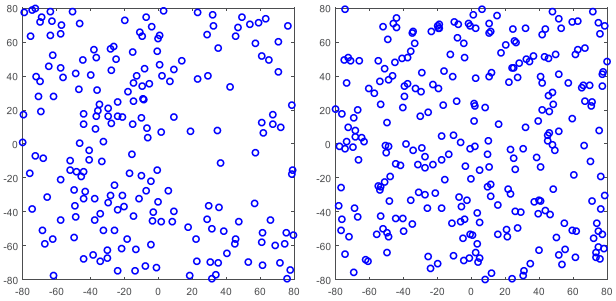

Fig. 2. Comparison of the BEPP (left) and PPP (right) with $N_\mathrm{p} = N_\mathrm{d} = 16$, $\xi = 2$, and other parameters are set to their default values in Table I. For both point processes, the density is 0.008.

Table I summarizes the notations of the parameters in the system model with their descriptions, and default values are given where applicable.

III. Analytical Results for the BEPP

In this section, the analytical results for the first- and second-order statistics are provided to characterize the BEPP.

A. The Density of the BEPP

Denoting by λ_e the density of the BEPP, we have $\lambda_\mathrm{e} = P_\mathrm{s}\lambda_\mathrm{p}$, where P_s is the probability of successful energy harvesting of a RF-powered node. Considering the typical RF-powered node at the origin, we have $P_\mathrm{s} = \mathbb{P}(E(o, \Phi_\mathrm{p}) = 1)$. In the following, we first give a complex yet highly accurate result on the density of the BEPP by considering the aggregate energy harvesting from all the RF transmitters. Next, a simple yet effective bound is proposed by merely considering the associated RF transmitter.

Theorem 1. *Let* $\delta \triangleq 2/\alpha$, $\tilde{R} \triangleq \min\{R_\mathrm{B}, (G_1/\xi)^{1/\alpha}\}$, $j \triangleq \sqrt{-1}$ *and*

$$\tilde{P}_\mathrm{s}(\xi) \triangleq 1 - \frac{1}{2}\Big(e^{-(13/10)\lambda_\mathrm{p}\pi\tilde{R}^2} + e^{-(13/10)\lambda_\mathrm{p}\pi R_\mathrm{B}^2}\Big) + \int_{\tilde{R}}^{R_\mathrm{B}}\int_0^\infty \frac{f(r)}{\pi t}\Im\Big(e^{-jt(\xi - G_1 r^{-\alpha}) - \lambda_\mathrm{p}\pi(R_\mathrm{B}^2 - r^2)(1-\varrho(t))}\Big)\mathrm{d}t\mathrm{d}r, \tag{12}$$

where $\Im(z)$ *denotes the imaginary part of* $z \in \mathbb{C}$, *and*

$$\varrho(t) = \sum_{i=1}^{4} \frac{q_i\delta(-jtG_i)^\delta}{R_\mathrm{B}^2 - r^2}\Big(\gamma(-\delta, \frac{-jtG_i}{r^\alpha}) - \gamma(-\delta, \frac{-jtG_i}{R_\mathrm{B}^\alpha})\Big). \tag{13}$$

The success probability of mm-wave energy harvesting is approximated by $P_\mathrm{s} \approx \tilde{P}_\mathrm{s}(\xi)$.

Proof: Letting $I_o = \sigma_{y\in\Phi_{\rm p}^!} G_y \ell(y)$ and $\tilde{\xi}(r) = \xi - G_1 r^{-\alpha}$, the success probability of the energy harvesting for the typical RF-powered node is given by

$$\begin{aligned} P_{\rm s} &= \mathbb{E}\Big[\mathbb{P}\big(I_o \geq \tilde{\xi}(r)\big) \mid y_0\Big] \\ &\overset{(a)}{\approx} \int_0^{R_{\rm B}} f(r)\Big[\mathbf{1}_{\tilde{\xi}(r)\leq 0} + \mathbf{1}_{\tilde{\xi}(r)>0}\,\mathbb{P}\big(I_o \geq \tilde{\xi}(r)\big)\Big]{\rm d}r \\ &= \underbrace{\int_0^{\tilde{R}} f(r){\rm d}r}_{\mathcal{A}_1} + \underbrace{\int_{\tilde{R}}^{R_{\rm B}} f(r)\mathbb{P}\big(I_o \geq \tilde{\xi}(r)\big){\rm d}r}_{\mathcal{A}_2}, \end{aligned} \tag{14}$$

where step (a) uses the approximative distance distribution in (4), and $\tilde{R} = \min\{R_{\rm B}, (G_1/\xi)^{1/\alpha}\}$. The first term $\mathcal{A}_1 = 1 - \exp\big(-(13/10)\lambda_{\rm p}\pi\tilde{R}^2\big)$ captures the contribution of the associated RF transmitter to the harvested energy, and the second term $\mathcal{A}_2$ captures the contribution from other RF transmitters if the energy harvested from the associated RF transmitter does not exceed the energy threshold.

To derive $\mathcal{A}_2$, we characterize the complementary cumulative distribution function of I_o given that $|y_0| = r$ via the conditional characteristic function of I_o, i.e., $\varpi(t) = \mathbb{E}(e^{jtI_o} \mid r)$. Due to the LOS ball model of mm-wave propagation, the contributors from other RF transmitters randomly and independently lie in the annulus with the outer radius $R_{\rm B}$ and inner radius r. Letting $N_{\rm c} \sim Poisson\big(\lambda_{\rm p}\pi(R_{\rm B}^2 - r^2)\big)$ be the number of RF transmitters lying in the annulus, the conditional Laplace transform of I_o is given by

$$\varpi(t) = \exp\big(-\lambda_{\rm p}\pi(R_{\rm B}^2 - r^2)(1 - \varrho(t))\big), \tag{15}$$

where $\varrho(t) = \mathbb{E}(e^{jtG_y\ell(y)})$. Since each of these RF transmitters uniformly lies in the annulus, the probability density function (PDF) of the distance between the RF transmitter and the origin is $\tilde{f}(x) = \frac{2x}{R_{\rm B}^2 - r^2}$, and we have

$$\begin{aligned} \varrho(t) &= \mathbb{E}\Big[\sum_{i=1}^{4} q_i e^{jtG_i\ell(y)}\Big] \\ &= \sum_{i=1}^{4} \frac{q_i\delta(-jtG_i)^{\delta}}{R_{\rm B}^2 - r^2}\Big(\gamma(-\delta, \frac{-jtG_i}{r^{\alpha}}) - \gamma(-\delta, \frac{-jtG_i}{R_{\rm B}^{\alpha}})\Big), \end{aligned}$$

where $\gamma(s,x) = \int_0^x t^{s-1}e^{-t}{\rm d}t$ is the lower incomplete gamma funciton. Through the Gil-Pelaez theorem, we have

$$\mathbb{P}(I_o \geq x) = \frac{1}{2} + \frac{1}{\pi}\int_0^{\infty} \frac{\Im\big(e^{-jtx}\varpi(t)\big)}{t}{\rm d}t. \tag{16}$$

Substituting (16) into (14), the final result is obtained. ∎

Since the numerical evaluation of the analytical expression in Thm. 1 is complicated, we further give a simpler approximation for the density of the BEPP by considering that the RF-powered node merely harvests energy from its associated RF transmitter in the following.

Corollary 1. *Letting* $\hat{P}_{\rm s}(\xi) \triangleq 1 - \exp\big(-(13/10)\lambda_{\rm p}\pi\tilde{R}^2\big)$, *the success probability of mm-wave energy harvesting is approximated as* $P_{\rm s} \approx \hat{P}_{\rm s}(\xi)$.

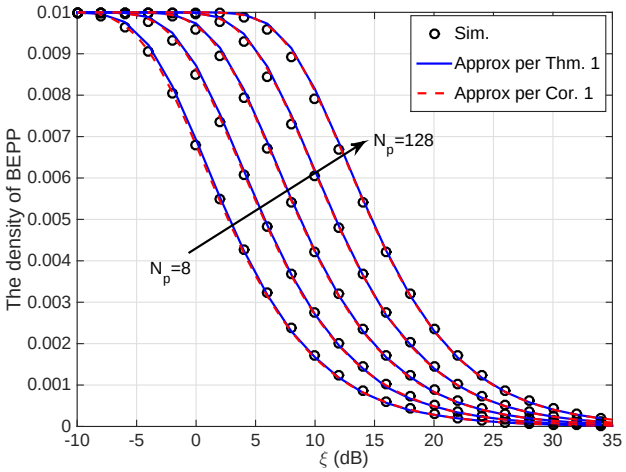

Fig. 3. The density of the BEPP versus ξ for $N_{\rm p} = 8, 16, 32, 64, 128$.

Fig. 3 shows the density of the BEPP with the comparison between the analytical and simulation results with $N_{\rm d} = 8$. We observe that the proposed two approximations match the simulation results quite well, which implies that the performance of energy harvesting is dominantly determined by the associated RF transmitter in mm-wave wirelessly powered networks.

B. The Pair Correlation Function of the BEPP

The pair correlation function (pcf) $g(r)$ [12, Def. 6.6] is usually used to characterize the spatial correlation, where r denotes the distance between two locations of the plane. Since the pcf of the BEPP is related to the statistics of the shapes of the Voronoi cells, it is difficult to derive an accurate expression and we resort to an asymptotic analysis and approximation as $r \to 0$. For notational convenience, we let $g(r) = \Theta(z(r))$ denote that $g(r)/z(r)$ tends to a positive constant in the limit indicated, and for $x \in \Phi_{\rm e}$, $p_x \in \Phi_{\rm p}$ denotes the RF transmitter of the Voronoi cell that x resides in.

Theorem 2. *When* $\Phi_{\rm p}$ *is a homogeneous PPP of density* $\lambda_{\rm p}$,

$$g(r) \sim c\lambda_{\rm p}^{1/2}P_{\rm s}^{-1}r, \quad r \to 0, \tag{17}$$

where c *is a constant that does not depend on* $\lambda_{\rm p}$, $P_{\rm s}$, *and* r.

Proof: According to [12, Def. 6.8], Ripley's K function is defined as $K(r) = \frac{1}{\lambda}\mathbb{E}_o^!\Phi\big(b(o,r)\big)$, where $\mathbb{E}_o^!$ is the expectation w.r.t. the reduced Palm measure. The pcf is

$$g(r) = \frac{1}{2\pi r}\frac{\rm d}{{\rm d}r}K(r) = \frac{1}{2\lambda\pi r}\frac{\rm d}{{\rm d}r}\mathbb{E}_o^!\Phi\big(b(o,r)\big). \tag{18}$$

Condition $\Phi_{\rm e}$ to have a point at the origin o. Denote by D_o the distance from o to the nearest boundary of the Voronoi cell V_{p_o}, and let $y \in \Phi_{\rm d}$ be the RF-powered node located in the adjacent Voronoi cell across that boundary. For $r \to 0$, $\Phi_{\rm e} \cap b(o,r)$ is either $\{o,y\}$ or $\{o\}$, and thus $\mathbb{E}_o^!\Phi\big(b(o,r)\big)$ equals the conditional probability of the joint event $\Phi_{\rm e} \cap b(o,r) = \{o,y\}$ and y succeeds in energy harvesting given that $o \in \Phi_{\rm e}$. Similar

to the proof of [8, Lemma 1], we have

$$\mathbb{E}_o^!\Phi\big(b(o,r)\big) \sim \mathbb{E}\left(\frac{r|\partial V_{p_o}|}{|V(p_o)|}\frac{S(D_o,r)}{|V(p_y)|}\frac{P_{\text{joint}}(o,y\mid\Phi_\text{p})}{\mathbb{P}(\varepsilon(o,\Phi_\text{p})\geq\xi\mid\Phi_\text{p})}\right),\ r\to 0, \quad (19)$$

where ∂V_{p_o} is the boundary of V_{p_o}, $|\partial V_{p_o}|$ and $|V_{p_o}|$ denote the perimeter and area of V_{p_o}, respectively, $S(D_o,r)$ is the area of the disk segment $b((-D_o,0),r)\cap(\mathbb{R}^+\times\mathbb{R})$, and $P_{\text{joint}}(o,y\mid\Phi_\text{p})$ denotes the joint success probability that both the two points at locations y and o succeed in energy harvesting. For $r\to 0$, y and o approach the common boundary of V_{p_o} and V_{p_y}, and $|p_o-o|$ tends to $|p_y-y|$. Hence, we have $P_{\text{joint}}(o,y\mid\Phi_\text{p})\sim\mathbb{P}(\varepsilon(o,\Phi_\text{p})\geq\xi\mid\Phi_\text{p})$ with $r\to 0$, and further obtain

$$\mathbb{E}_o^!\Phi\big(b(o,r)\big)\sim\mathbb{E}\left(\frac{r|\partial V_{p_o}|}{|V(p_o)|}\frac{S(D_o,r)}{|V(p_y)|}\right),\ r\to 0. \quad (20)$$

Since $S(D_o,r)=\Theta(r^2)$, the area and perimeter of the Voronoi cell scale with λ_p and $\sqrt{\lambda_\text{p}}$, respectively, and the expectation over the Φ_p does not affect the exponent of r and the scaling law of λ_p, we have $\mathbb{E}_o^!\Phi\big(b(o,r)\big)=\lambda_\text{p}^{3/2}\Theta(r^3)$, $r\to 0$, and

$$g(r)=\frac{1}{2\pi\lambda_\text{p}P_\text{s}r}\frac{\text{d}}{\text{d}r}\left[\lambda_\text{p}^{3/2}\Theta(r^3)\right]\sim c\lambda_\text{p}^{1/2}P_\text{s}^{-1}r,\ r\to 0, \quad (21)$$

where c is a constant, independent of λ_p, P_s, and r. ■

To obtain a concrete $g(r)$, we further assume that the Voronoi cells of RF transmitters are square-shaped and their areas are independently gamma-distributed variables with PDF [13]

$$f_A(x)=\frac{3.5^{3.5}}{\Gamma(3.5)}\lambda_\text{p}^{3.5}x^{2.5}e^{-3.5\lambda_\text{p}x}. \quad (22)$$

Hence, we have

$$\mathbb{E}_o^!\Phi\big(b(o,r)\big)\ \simeq\ \mathbb{E}\left(\frac{r|\partial V_{p_o}|}{|V(p_o)|}\right)\mathbb{E}\left(\frac{S(D_o,r)}{|V(p_y)|}\right) \overset{(a)}{\simeq}\ \frac{9\sqrt{\lambda_\text{p}}r}{2}\times\frac{14}{15}\lambda_\text{p}r^2,\ r\to 0, \quad (23)$$

where $\simeq$ denotes an approximation that becomes better asymptotically and step (a) follows from the same reasoning as in [8], and we further obtain

$$g(r)\simeq 2\lambda_\text{p}^{1/2}P_\text{s}^{-1}r,\ r\to 0, \quad (24)$$

i.e., the constant c in (17) is approximately 2.

Fig. 4 illustrates simulations and fitted functions of the pcfs with $N_\text{p}=16$ and $N_\text{d}=8$, where the fitted functions include

$$\tilde{g}(r)=1-e^{-a\sqrt{\lambda_\text{p}}r/P_\text{s}}+b(\sqrt{\lambda_\text{p}}r/P_\text{s})^2e^{-c(\sqrt{\lambda_\text{p}}r/P_\text{s})^2}, \quad (25)$$

and the one in (3). It is observed that the pcfs are first smaller and then larger than in the PPP case ($g(r)=1$) and finally tends to the PPP case with the increase of r, which demonstrates the correlation behavior of the active RF-powered nodes in a wide range of distances. Comparing the two fitting results per (25) and (3), the former fits well for both cases while the later only applies to certain cases with high probability of successful energy transfer. Specifically, for small r, the locations of the nodes exhibit obvious repulsion.

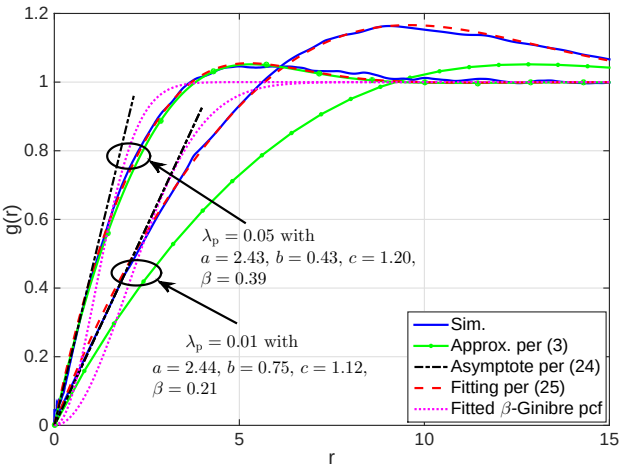

Fig. 4. The pcfs of the BEPP with different λ_p.

Since the β-GPP [7] has been widely used as a model with repulsion, we also use a fitted β-GPP to approximate the BEPP with the pcf function as

$$g_\text{gin}(r)=1-\exp(-\lambda_\text{p}P_\text{s}\pi r^2/\beta). \quad (26)$$

It turns out that the repulsive behavior at a small r can be exactly captured by the fitted β-GPP through moment matching. In contrast, as r increases, the repulsive correlation weakens and clustering occurs instead.

IV. Information Transmission Performance

The performance of the information transmission is highly correlated to the spatial distribution of the BEPP. Conditioning on that the typical RF-powered node is at the origin, we focus the success probability of the typical receiver at $z=(r_\text{d},0)$. Letting $\Phi_\text{e}^!=\Phi_\text{e}\setminus\{o\}$ and $I(z)=\sum_{x\in\Phi_\text{e}^!}G_{xz}\ell(x-z)h_{xz}$ be the interference at the typical receiver, the (received) signal-to-interference ratio (SIR) is

$$\text{SIR}=G_1r_\text{d}^{-\alpha}h_{oz}/I(z), \quad (27)$$

and the success probability is defined as $P(\theta)\triangleq\mathbb{P}(\text{SIR}>\theta)$ where θ is the SIR threshold. With Rayleigh fading, we have $P(\theta)=\mathcal{L}_{I(z)}(\theta r_\text{d}^\alpha G_1^{-1})$, where

$$\mathcal{L}_{I(z)}(s)=\mathbb{E}\exp\Big(-s\sum_{x\in\Phi_\text{e}^!}G_{xz}\ell(x-z)h_{xz}\Big) =\mathbb{E}_o^!\Big(\prod_{x\in\Phi_\text{e}}\sum_{i=1}^{4}\frac{q_i}{1+sG_i\ell(x-z)}\Big). \quad (28)$$

Hence the success probability is given by the reduced Palm distribution of the BEPP, and thus an exact calculation seems unfeasible. Thus next, we approximate it with common point processes through the first- and second-order statistics.

1) PPP Approximation: We first use a PPP with density λ_s to approximate the BEPP. From Slivnyak's theorem [12], the reduced Palm distribution is the same as the original distribution. Due to the PPP approximation, the interference at

z is equally distributed as that at the origin and hence, $\mathcal{L}_{I(z)}(s)$ can be approximated by

$$\mathcal{L}_{I_{\rm PPP}}(s)=\exp\Big(-2\pi\lambda_{\rm e}\sum_{i=1}^{4}q_i\int_0^{R_{\rm B}}\frac{r{\rm d}r}{1+(sG_i)^{-1}r^{\alpha}}\Big), \quad (29)$$

where the integral upper limit is obtained by the path loss function in (6).

2) β-GPP Approximation: Since $g(r)\neq 1$, the PPP approximation is inaccurate. Thus we provide another approximation of the BEPP with a fitted β-GPP using the first- and second-order statistics. Since the typical receiver is located at z, the interfering RF-powered nodes lie in $b(z,R_{\rm B})$ per the path loss function in (6). Hence, using the Palm measure and the properties of β-GPPs [7], $\mathcal{L}_{I(z)}(s)$ is approximated by

$$\mathcal{L}_{I_{\rm gin}}(s)=\prod_{k=2}^{\infty}\Big(1-\beta+\beta\sum_{i=1}^{4}q_i\int_0^{\infty}\frac{(\frac{\lambda_{\rm e}\pi}{\beta}r)^k e^{-\frac{\lambda_{\rm e}\pi r}{\beta}}{\rm d}r}{\Gamma(k)r(1+sG_i r^{-\frac{\alpha}{2}})}\Big). \quad (30)$$

Fig. 5 illustrates the success probabilities with PPP and β-GPP approximations for different $\lambda_{\rm p}$. It is observed that the β-GPP-based results match the simulation results extremely well, while PPP approximation shows obvious deviations. The reason is that the higher-order statistics of the BEPP strongly affect the information transmission performance. Therefore, compared with the PPP, the β-GPP is a more suitable model for capturing such repulsion of the energized nodes via directed mm-wave energy transfer.

V. Conclusions

This paper considered a mm-wave wirelessly powered network, where the RF transmitters employed a directed energy transfer policy and each RF-powered node harvested energy from its nearest RF transmitter. Due to the directed energy transfer, the harvested energy from different RF transmitters is correlated, which determines the properties of the point process of nodes (the BEPP) that successfully harvest enough energy. Within a stochastic geometry-based framework, we derived the first- and second-order statistics for the BEPP, respectively. The results indicate that (1) with directed energy transfer, the energized nodes exhibit repulsive behavior at small distances which gradually wears off with increasing distance; (2) as the distance increases, the energized nodes exhibit a clustering behavior. Furthermore, we compared the widely-used PPP approximation with the β-GPP approximation to the BEPP, and the results show that the transmission success probability via the β-GPP approximation coincides quite exactly with the simulation curves. Overall, both the analysis and approximation show that the energy correlation caused by the directed energy transfer has a non-negligible impact on the communication performance.

Acknowledgment

The work of N. Deng has been supported by National Natural Science Foundation of China (61701071), the China Postdoctoral Science Foundation (2017M621129 and 2019T120204), the open research fund of National Mobile Communications Research Laboratory, Southeast University (No. 2019D03), the Fundamental Research Funds for the Central Universities (DUT19RC(4)014), and the work of M. Haenggi has been supported by the U.S. NSF (grant CCF 1525904).

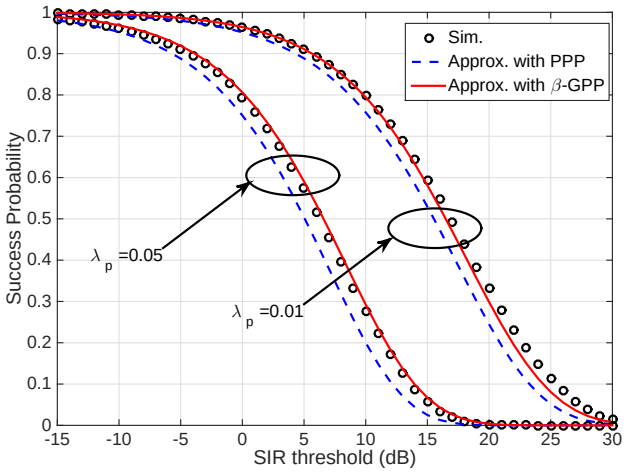

Fig. 5. The success probability with PPP and β-GPP approximations.

References

[1] M. R. Akdeniz, Y. Liu, M. K. Samimi, S. Sun, S. Rangan, T. S. Rappaport, and E. Erkip, "Millimeter wave channel modeling and cellular capacity evaluation," *IEEE Journal on Selected Areas in Communications*, vol. 32, no. 6, pp. 1164–1179, Jun. 2014.

[2] L. Wang, K. Wong, R. W. Heath, and J. Yuan, "Wireless powered dense cellular networks: How many small cells do we need?" *IEEE Journal on Selected Areas in Communications*, vol. 35, no. 9, pp. 2010–2024, Sep. 2017.

[3] X. Zhou, J. Guo, S. Durrani, and M. Di Renzo, "Power beacon-assisted millimeter wave ad hoc networks," *IEEE Transactions on Communications*, vol. 66, no. 2, pp. 830–844, Feb 2018.

[4] N. Deng and M. Haenggi, "The energy and rate meta distributions in wirelessly powered D2D networks," *IEEE Journal on Selected Areas in Communications*, vol. 37, no. 2, pp. 269–282, Feb. 2019.

[5] T. A. Khan and R. W. Heath, "Wireless power transfer in millimeter wave tactical networks," *IEEE Signal Processing Letters*, vol. 24, no. 9, pp. 1284–1287, Sep. 2017.

[6] N. Deng and M. Haenggi, "Energy correlation in wirelessly powered networks," in *2019 IEEE International Conference on Communications (ICC)*, Shanghai, May 2019.

[7] N. Deng, W. Zhou, and M. Haenggi, "The Ginibre point process as a model for wireless networks with repulsion," *IEEE Transactions on Wireless Communications*, vol. 14, no. 1, pp. 107–121, Jan. 2015.

[8] M. Haenggi, "User point processes in cellular networks," *IEEE Wireless Communications Letters*, vol. 6, no. 2, pp. 258–261, April 2017.

[9] J. G. Andrews, T. Bai, M. N. Kulkarni, A. Alkhateeb, A. K. Gupta, and R. W. Heath, "Modeling and analyzing millimeter wave cellular systems," *IEEE Transactions on Communications*, vol. 65, no. 1, pp. 403–430, Jan. 2017.

[10] X. Yu, J. Zhang, M. Haenggi, and K. B. Letaief, "Coverage analysis for millimeter wave networks: The impact of directional antenna arrays," *IEEE Journal on Selected Areas in Communications*, vol. 35, no. 7, pp. 1498–1512, Jul. 2017.

[11] N. Deng, M. Haenggi, and Y. Sun, "Millimeter-wave device-to-device networks with heterogeneous antenna arrays," *IEEE Transactions on Communications*, vol. 66, no. 9, pp. 4271–4285, Sep. 2018.

[12] M. Haenggi, *Stochastic geometry for wireless networks*. Cambridge University Press, 2012.

[13] J.-S. Ferenc and Z. Néda, "On the size distribution of Poisson Voronoi cells," *Physica A: Statistical Mechanics and its Applications*, vol. 385, no. 2, pp. 518–526, 2007.